INTERNATIONAL JOURNAL OF PLANT, ANIMAL AND ENVIRONMENTAL SCIENCES

IJPAES

Volume-6, Issue-2, April-June-2016 Coden: IJPAJX-CAS-USA, Copyrights@2015 ISSN-2231-4490

Received: 1st Sep-2015 ***Revised: 19th Oct-2015*** ***Accepted: 26th Nov-2015***

Research article

CHARACTERIZATION AND USE OF A CUBAN MINERAL IN ELIMINATION OF CRYSTAL VIOLET FROM AQUEOUS SOLUTION

Heidy Fernández-Hechevarría[1], Juan A Cecilia[2], María I. Garrudo-Guirado[1], Juan M. Labadie-Suarez[1], José L. Contreras-Larios[3], Miguel A. Autie-Pérez[1,2] and Enrique Rodríguez-Castellón[2*]

[1]Departamento FQB. Facultad de Ingeniería Química. Instituto Superior Politécnico José Antonio Echeverría. MES, Habana, Cuba.

[2]Andalucía Tech,Departamento de Química Inorgánica, Cristalografía y Mineralogía, Facultad de Ciencias, Universidad de Málaga, España.

[3]Departamento de Energía de la Universidad Autónoma Metropolitana- Azcapotzalco CBI Energía. México D.F., México.

ABSTRACT: A Cuban mineral was used to evaluate its adsorption capacity in the removal of crystal violet (CV) from aqueous solutions. The mineral was characterized by several physicochemical techniques. Both N_2 adsorption-desorption isotherm at 77K, fitted with the Brunnauer–Emmet–Teller model, and the results of the average pore distribution revealed that the Cuban mineral used in this study is a mesoporous material. The FTIR spectrum indicated a high content of carbonate species; however, the XPS spectrum also revealed the presence of silicon species on the surface of the adsorbent, which suggests the coexistence both carbonate and silicate species in the raw material. The efficiency for CV removal, the role of the contact time and of the initial concentrations of the adsorbate were evaluated in this study. The adsorption kinetic was fitted with the pseudo second order model. This result indicated that the adsorption mechanism was through chemisorption process between CV and Cuban mineral. The results showed that CV adsorption isotherm was best described by the Langmuir model. The adsorption capacity for CV was 55.63 mg/g. The abundant deposits, low cost and easy access make of mineral SAN1 a good natural adsorbent to treat large volumes of dye polluted waters.

Key words: Contamination, Adsorption; Crystal violet; Cuban mineral

*Corresponding author: Enrique Rodríguez-Castellón, Andalucía Tech, Departamento de Química Inorgánica, Cristalografía y Mineralogía, Facultad de Ciencias, Universidad de Málaga, España.Email: castellón@uma.es

INTRODUCTION

The growth of world population has led to the consumption of water is doubling every twenty years. This fact requires improving the treatment of domestic water and wastewater. Thus, wastewaters generated by industrial and domestic activities have also increased, but only around 5% are treated to be recycled. Data reported by the United Nations show that one in five people worldwide lacks access to safe drinking water, while some 2.4 billion lack adequate sanitation [1]. The textile industry consumes large quantities of water and produces large volumes of wastewater in various stages of the processes of dyeing and finishing of the tissues, with high emissions of colored organic compounds. The dyes when are present in wastewater are discharged into water, even at low concentrations, producing an intense color that brings a strong environmental impact, not only for its visual pollution, but rather for its toxicity [2].

The CV is widely used for dyeing in textile industry, in the manufacture of paints and printing inks. Moreover, CV is the active ingredient of Gram stain, and it is also used as an antibacterial agent in humans [3]. Furthermore, CV is used as an additive to poultry feed to inhibit mold growth, intestinal parasites and fungi. On the contrary, this dye is liable to cause moderate eye irritation, it is highly toxic for mammalian cells and it is harmful by adsorption causing irritation of the skin and digestive tract. In extreme cases, CV can cause respiratory and renal failure, being classified as a recalcitrant molecule [4].

For the above and because of the structural complexity of conventional treatment plants for decreasing pollution load of wastewater, it is reported in the literature that only a low percentage of dyes is removed, suggesting that many of these wastewaters are discharged without treatment [5]. Some chemical and physical methods, such as coagulation, flocculation and sonication have been used for the wastewater treatment; however the most of these processes have several disadvantages such as the high operating costs and the need for specialized equipment [6] which limits its implantation.

Adsorption is an alternative process, with great prospects for the treatment of wastewater containing dyes. Activated carbon (AC) is typically used to retain organic molecules; however, its regeneration increases the costs of its use for the development countries. Nowadays, it is important the development of inexpensive adsorbent materials and easily available to minimize the amount of organic compounds in wastewater. Several low cost adsorbents have been proposed for dye removal such as modified magnetic calcium ferrite nanoparticles [7], bentonite [8], kaolin [9], papaya seeds [10], and orange peel [11], among others.

Sama are deposits of non-metallic Cuban minerals located in the eastern region which have been scarcely studied. These deposits have mainly used to the cement industry, while its use in the ceramic industry or the manufacturing of prefabricated elements has been lesser extended. For these reasons, this mineral has a low economic value, which together with its physical and chemical properties could provide a great potential for the treatment of liquid and gaseous waste, drinking water treatment and filtering of water for human consumption [12]. Its use as an adsorbent material would add great economic value, and most importantly, provide an inexpensive adsorbent compared to the traditional materials used in the wastewater treatment.

The aim of this work is the determination of physical and chemical properties of the Sama mineral. For this purpose, N_2 adsorption-desorption at 77 K, X-ray diffraction (XRD), Fourier transform infrared spectroscopy (FTIR), X-ray photoloelectron spectroscopy (XPS) were carried out. In addition, the adsorption capacity of this material was evaluated in the removal of CV from aqueous solutions by the fitting of the experimental data to adsorption isotherms and sorption kinetics.

MATERIALS AND METHODS

Adsorbent material

The mineral obtained from the Sama deposits was milled and sieved. The fraction used in this work was in the ranging of 0.10-0.25 mm. The mineral was labeled as SAN1. The material was used in its raw form and another fraction was modified with an acid treatment (HCl 1M), being labeled as SAN1Q. Both samples were tested for CV removal from aqueous solutions in a batch process.

Crystal Violet (CV) solution

CV (CI 42555, λ_{max}: 590 nm, molecular weight: 407.99 g/mol, and molecular formula: $C_{25}H_{30}N_3Cl$, 99% purity) was purchased from MERCK. A stock solution of CV (1000 ppm) was prepared and suitably diluted to the required initial concentrations. The concentrations of the dye in stock solutions and all samples during the experimental tests were measured using a Shimadzu UV-1800 spectrophotometer.

Characterization

Chemical Composition

The chemical composition of the sample was determined by energy dispersive X-ray fluorescence spectroscopy, using a Shimadzu EDX-800HS spectrometer with Rh target X-ray tube. The X-ray tube was operated at 50 kV and 30 mA. The measurements were performed in air. The measurement time for each element was 100s.

IR spectroscopy

Infrared (IR) spectra were carried out in the 4000–350 cm^{-1} range with a resolution of 2 cm^{-1} and 20 scans for each adsorbent, at room temperature, using a Shimadzu IRPrestige-21 FTIR attenuated total reflection (ATR).

Diffraction X-ray powder (XRD)

SAN1 and SAN1Q diffractograms were obtained at room temperature, using a diffractometer Shimadzu XRD-7000 Maxima X, with Cu Kα radiation X-ray tube. The samples were run on a range of 5 to 120º with a step of 0.02 degrees. The X-ray tube was operated at 30 kV and 30 mA.

Surface area, BET (S_e), and pore size distribution

The textural properties of the adsorbents were evaluated using the N_2 adsorption-desorption at 77 K in a Micromeritics ASAP 2020 V3.03 E by the fitting of the adsorption isotherms to the Brunauer–Emmett–Teller (BET) equation. Porosity determinations were performed with a Carlo Erba Mercury Porosimeter (MP) Model 1800 Sortomatic which allowed calculation of the meso- and macroporosity of the raw mineral, through the volume of mercury entered into the pores with radio between 7500 and 9.4nm (Dp = 15000-18.8 nm).

X-ray photoelectron spectroscopy

X-ray photoelectron spectra were collected using a Physical Electronics PHI 5700 spectrometer with non-monochromatic Mg Kα radiation (300 W, 15 kV, and 1253.6 eV) with a multi-channel detector. Spectra of the samples were recorded in the constant pass energy mode at 29.35 eV, using a 720 µm diameter analysis area. Charge referencing was measured against adventitious carbon (C 1*s* at 284.8 eV). A PHI ACCESS ESCA-V6.0 F software package was used for acquisition and data analysis. A Shirley-type background was subtracted from the signals. Recorded spectra were always fitted using Gaussian–Lorentzian curves in order to determine the binding energies of the different element core levels more accurately. The samples were directly analyzed without previous treatment.

Adsorption kinetics

The kinetic analyses of adsorption processes were carried out as follows: A given amount of adsorbent (SAN1 or SAN1Q) was put in contact with 50 mL of a CV solution of 50 mg/L as initial concentration. Each mixture was placed in a glass bottles and stirred at different times (5, 10, 15, 20, 25, 30, 35, 40, 45, 50, 55 and 60 min) at 120 rpm and room temperature. After that, each sample was filtered. Batch experiments were repeated at least three times to ensure the accuracy of the obtained data. The CV concentrations in the solutions were determined using Shimadzu UV-1800 spectrophotometer at a wavelength corresponding to the maximum absorbance, λ=590 nm. In order to elucidate the adsorption mechanism, the adsorption data were fitted to pseudo-first-order, pseudo-second-order and second-order models.

Pseudo-first-order: This model is commonly used for homogeneous adsorbents and physical adsorption, the adsorption rate is proportional to the solute concentration [13]. It is represented by equation (1):

$$log(q - q_e) = log q_e - \frac{k_1 t}{2.303} (1)$$

where: q_e is the amount of dye retained in the balance (mg/g), q the amount of solute adsorbed per unit of weight of adsorbent (mg/g) and k_1 is the pseudo first order adsorption rate constant (min $^{-1}$).

Pseudo-second-order: This model, represented by equation (2), assumes that the rate limiting stage may be chemisorption, involving valence forces through the sharing or exchange of electrons between adsorbent and adsorbate [14]

$$\frac{t}{q} = \frac{1}{k_2 {q_e}^2} + \frac{t}{q_e} (2)$$

where q_e is the amount of dye retained in the balance (mg/g), q the amount of solute adsorbed per unit weight of adsorbent (mg/g) and k_2 is the pseudo-second order adsorption rate constant (g/mg min).

Second-order:Elovich model represented by equation (3), of general application in chemisorption processes, assumed that the active sites of the adsorbent are heterogeneous and therefore exhibit different activation energies, based on a reaction mechanism of second order heterogeneous reaction process [15]

$$q = \frac{ln\,(ab)}{b} + \frac{ln\,(t)}{b} (3)$$

where a is the constant of adsorption (mg/g) and *b* is the constant of desorption (g/mg).

Adsorption Isotherms

Adsorption isotherm studies were carried with SAN1 and SAN1Q adsorbents by batch equilibrium technique. A given amount of adsorbent was set in contact with 50 mL of a solution of the dye at different concentrations during the equilibrium time at room temperature. CV concentrations were determined in the liquid phases as described above. The dye adsorption capacity was calculated by using equation (4):

$$Q_{ads} = \frac{(C_i - C_{eq})V}{m} (4)$$

where Q_{ads} is the number of solute adsorbed per unit of weight of adsorbent (mg/g), C_i is the initial concentration of dye in the CV solution (mg/L), C_{eq} is the CV equilibrium concentration of dye in the solution obtained after adsorption (mg/L), V is the volume of fluid removed after adsorption (L) and m is the mass of adsorbent used in each experimental point (g).

The experimental results were analyzed using adsorption models of Langmuir and Freundlich to determine the correlation between the solid phase and aqueous equilibrium concentrations.

Langmuir adsorption isotherm: This model assumes that the adsorption is limited to fill a single layer (monolayer) and there are no interactions between the adsorbed molecules with adjacent bonding sites [16, 17], and it is given by equation (5).

$$q_e = \frac{k_L q_{max} C_{eq}}{1 + k_L C_{eq}} (5)$$

whereq_e is the amount of solute adsorbed per unit of weight of adsorbent (mg/g), q_{max} is the maximum adsorption capacity (mg/g), C_{eq} is the concentration of solute in the liquid at equilibrium (mg/L), k_L the saturation constant (mg/L) related to the energy or net enthalpy of adsorption.

The essential characteristics of the Langmuir isotherm can be expressed in terms of separation factor [18] or what is the same, the balance parameter ($R_{L,}$ dimensionless), which is defined by equation (6).

$$R_L = \frac{1}{1 + K_L C_{eq}} (6)$$

whereK_L is the Langmuir constant and C_{eq} is the concentration of the dye in the solution after the adsorption.

According to the value of R_L,the shape of the isotherm can be interpreted as follows: If R_L>1, the adsorption is not favorable; if R_L=1, adsorption is linear; if 0<R_L<1, adsorption is favorable and if R_L=0, the adsorption is irreversible.

Freundlich adsorption isotherm: This model, represented by equation (7), assumes surface heterogeneity and exponential distribution of active sites, it provides an empirical relationship between the adsorption capacity and constant balancing of the adsorbent [19].

$$q_e = k_f C_{eq}^{\frac{1}{n}} (7)$$

whereq_e is the amount of solute adsorbed per unit of weight of adsorbent (mg/g), C_{eq} is the concentration of solute in the liquid at equilibrium (mg/L), k_f Freundlich constant (mg/g) and *1/n* Freundlich coefficient which is indicative of the heterogeneity of the adsorbent surface.

RESULTS AND DISCUSSIONS

Chemical Composition

The results of chemical analysis, estimated by X-ray fluorescence spectroscopy, show the predominance of calcium, silicon and aluminum. In addition, other elements as alkaline, alkaline earth metals and heavy metals appear in smaller proportions. These data reveal that the main mineralogical phases must involve the presence of calcium and silicon species (Table 1).

Table 1: Chemical Composition of SAN (Metal Oxides in wt %)

K_2O	Fe_2O_3	Na_2O	CaO	SiO_2	MgO	TiO_2	Al_2O_3
0.33	1.07	0.02	42.22	17.71	0.46	0.1	2.26

IR spectroscopy

The IR spectrum of natural mineral (Figure 1A) shows bands with vibration frequencies in the range of 700-1500 cm^{-1}, which confirms the presence of carbonate species as main mineralogical phase. These bands located at: 713 cm^{-1} (v_4), 1420 cm^{-1} (v_3), 877 cm^{-1} (v_2) and 1087 cm^{-1} (v_1) have been assigned to the internal vibration modes of the carbonate ion CO_3^{2-} in the form of calcium carbonate [20-22]. Besides the internal vibration modes, the combination of previous bending modes such as (v_4+ v_1) at 1800 cm^{-1}, (v_3+ v_1) at 2510 cm^{-1} and 2v_3 at 2840 cm^{-1} have also been detected [22,23]. Finally, the band with a maximum located at 3400 cm^{-1} has been attributed to H-bonded water of the humidity of the calcite [24].

In addition, it has been detected a band at 1007 cm^{-1} with a shoulder at 1180 cm^{-1} assigned to Si-O stretching and Si-O stretching (longitudinal mode) together with a band about 790 cm^{-1} which is attributed to Al-O-Si in-plane vibration [25]. The band located at 1639 cm^{-1} is attributed to the bending vibration of the water.

The wide band in the range of 3525–3000 cm^{-1} was assigned to the overlapping of the O–H stretching band of hydrogen-bonded water molecules (H–O–H) and SiO–H stretching mode of the hydrogen of surface silanol bonded to molecular water (SiO–O···H_2O). The sharp band located at above 3600 cm^{-1} can be assigned to the symmetrical stretching vibration mode of O–H from isolated terminal silanol groups [25]. In order to ensure that the bands located between 2980-2870 cm^{-1} do not belong to C-H stretching, the SAN mineral was calcined at 400 ºC for 4 hours, remaining these bands which confirms that these bands are attributed to the combination of bending modes of carbonate species of $CaCO_3$ (Figure 1B).

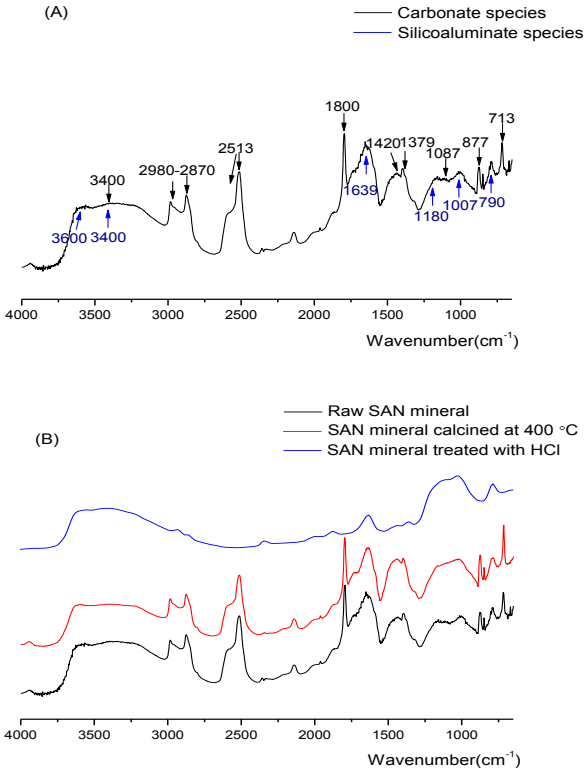

Figure 1: IR spectrum of mineral SAN1 (A) and comparative of IR spectra before and after the calcination at 400ºC.

X-ray diffraction (XRD)

The diffractogram of SAN (Figure 2) shows well-defined diffraction peaks of $CaCO_3$ ascribed to calcite species ($CaCO_3$) (Ref: 98-005-2151) [26]. The calcite particle size was estimated by using the Williamson-Hall method with a fitting of the diffraction profile, obtaining a crystal size of 134 nm. In addition, it is noticeable the existence of other mineralogical phases in minor proportion and/or with lower particle size than calcite.

Thus, the diffractogram shows the presence of silica (SiO_2) in the form of quartz, located at 2θ = 26.6º (Ref: 01-079-1915), magnesium carbonate ($MgCO_3$) in the form of magnesite (Ref: 98-004-0117), located at 2θ = 32.6º, magnesium oxide (MgO) in the form of periclase located at 2θ = 42.2º (Ref: 96-900-6761) and several feldspars such as albite (Ref: 98-005-2343) and anhortite (Ref: 00-041-1481) located between 2θ = 20 and 30º.

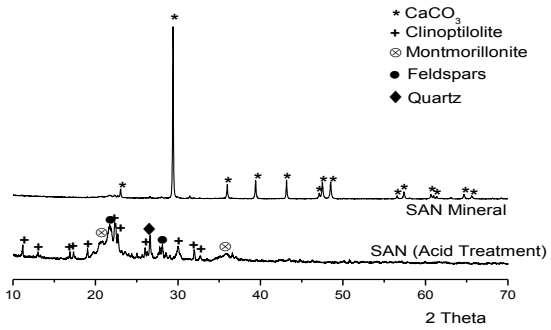

Figure 2: Diffractograms of SAN1 mineral SAN1Q mineral treated with HCl

Surface area, BET (S_e), and pore size distribution

According to the IUPAC classification, the adsorption-desorption isotherm of N_2 at 77 K displays a type II isotherm [27], typical of non-microporous solids. The determination of specific surface area by the S_{BET} equation established a value of 41 m^2/g for the raw mineral (Figures 3A and 3B). This S_{BET} valueis low in comparison with those of other adsorbents used in dyes adsorption processes, such as activated carbon whose S_{BET} values are of order of hundreds of m^2/g [28]. However, the cost of this mineral as adsorbent is much lower than that of other porous materials.The mercury intrusion curve in SAN shows an abrupt initial rise, typical of the space between the particles filling (Figure 4). Approximately from 20 to 100 atm, the curve is remarkably bent which showed the presence of macropores with diameters between 750 and 150 nm. Between 100 and 800 atm, the slope varies slowly indicating that the volume of pores with diameters between 150 and 20 nm is low (less than 10% of total) and the volume of pores with diameters between 50 and 20 nm (mesopores) is also low (less than 6%, Table 2). From these results, it could be inferred that the mineral in its natural state, is a macro-mesoporous solid with predominance of macropores according to the classification of porosity by IUPAC [27]. It is noteworthy that the low value of S_e obtained by N_2 adsorption at 77 K is in correspondence with the porous properties obtained by MP.

Table 2: Total volume (V_T), Volume of pores with diameters lower than 50 nm (V<50nm), and volume of pores with diameters higher than 50 nm (V>50nm) obtained from mercury porosimetry.

Mineral	V_T (cm^3/g)	V<50nm (cm^3/g)	V>50nm (cm^3/g)
SAN	0.208	0.011	0.197

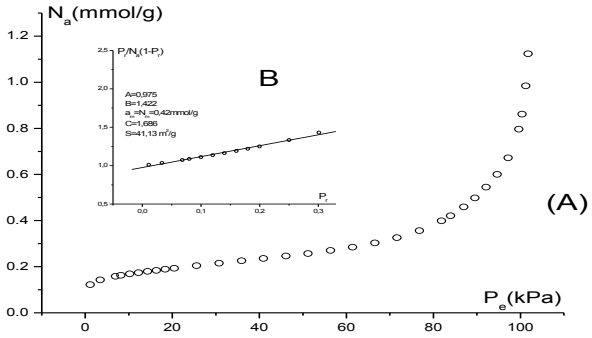

Figure 3: (A) Adsorption isotherm of N_2 at 77 K in SAN1 (B) its representation in BET's coordinates.

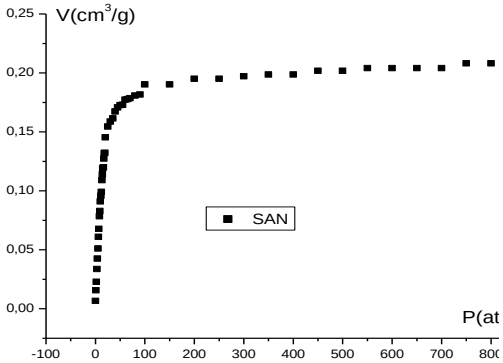

Figure 4: Mercury volume introduced as a function of pressure for SAN1 mineral.

X-ray photoelectron spectroscopy

XPS analysis was carried out to evaluate the surface composition of the adsorbent and the chemical state of their constituent elements. Table 3 shows the binding energy values (in eV) and the atomic concentration (%AC). The C 1*s* core level spectrum of the SAN spectrum can be decomposed in two contributions assigned to adventitious carbon and organic matter, both located at similar BE, about 284.8 eV, and carbonate species located at 289.4 eV, which is in agreement to that observed in the FTIR spectrum and XRD data (Figures 1 and 2). The O 1*s* core level signal shows a unique contribution located at 531.5 eV that can be ascribed to the presence of carbonate species and/or aluminosilicate species. The Ca $2p_{3/2}$ region displays a contribution located about 346.6 eV attributed to calcium (II) in the form of carbonate species.

With regard to the Si 2*p* region, the signal located at 102.7 eV is attributed to silicon species in the form of aluminosilicate. In the same way, the Al 2*p* region shows a band about 74.2-74.3 eV which is assigned to aluminosilicate. In addition, minor quantities of Mg and Fe were detected.

Table 3: Binding energy values of the constituent elements of SAN mineral before and after the adsorption process (SAN-VC) and their respective atomic concentrations (%) determined by XPS

Element	SAN		SAN-VC	
	Binding Energy (eV)	Atomic concentration (%)	Binding Energy (eV)	Atomic concentration (%)
C 1*s*	284.8	11.5	284.8	13.8
C 1*s*	-	-	287.2	1.0
C 1*s*	289.4	8.1	289.5	6.6
C 1*s* (Total)	-	19.6	-	21.4
O 1*s*	531.5	55.7	531.5	53.4
Si 2*p*	102.7	13.7	102.5	14.2
Al 2*p*	74.2	1.8	74.3	1.8
Ca 2*p*	346.9	7.6	347.1	6.5
Mg 2*p*	49.5	0.9	49.5	0.7
Fe 2p	711.9	0.7	711.7	1.0
N 1s	-	-	399.1	1.0

Obtainment of the calibration curve

The calibration curve has been obtained based on the absorbance against the concentration of CV in working solutions. Analyzing the values of the correlation (R=0.997) and determination (R^2=0.997) coefficients, it has been possible to infer the good correlation between the variables plotted.

Determining the minimum adsorption time

According to the form of the graphical Q_{ads}=f(t) of the adsorbed CV in SAN, the highest adsorbed amount (12.1 mg/g) was reached after 25 minutes of stirring, which was taken as the equilibrium time of the process for fixed experimental conditions.

The shape of the graph indicates that the adsorption process was divided into three stages: a first step where the amount adsorbed increases rapidly over time, perhaps due to the diffusion of CV from the solution to the surface of the adsorbent. A second stage where the process is very slow and a third stage in which Q_{ads} remains constant, indicating that the equilibrium has been reached (Figure 6).

The analysis of the results obtained by applying the kinetic models (Figure 7) indicates that the process adsorption is best described with the model of pseudo-second order model, which is able to assert that the adsorption process should occur due to valence forces through the exchange or sharing of electrons between the CV and SAN. This conclusion was based on the analysis of the correlation coefficient (R^2=0.994) (Table 4), in addition to the comparison between the experimental value of the amount of adsorbed dye and calculated value with each model.

Adsorption parameters on the model of second order were quite different; the rate of adsorption was 2.5×10^{-13} times smaller than the initial rate of dye adsorption; indicating that the affinity of CV for the binding sites of SAN is very high.

Table 4: Parameters calculated from the kinetic model used

Pseudo-First Order				
$q_{ecalc}(mg/g)$	$q_{eexp}(mg/g)$	$k_1(min^{-1})$	R^2	
12.028	12.118	0.542	0.725	0.163
Pseudo-Second Order				
$q_{ecalc}(mg/g)$	$q_{eexp}(mg/g)$	k_2 (g/mg min)	R^2	
12.226	12.118	0.84	0.994	0.011
Second Order				
$a(mg/g*min)$	$b(mg/g*min)$	R^2	SSE	
7.763×10^{13}	3.042	0.848	0.117	

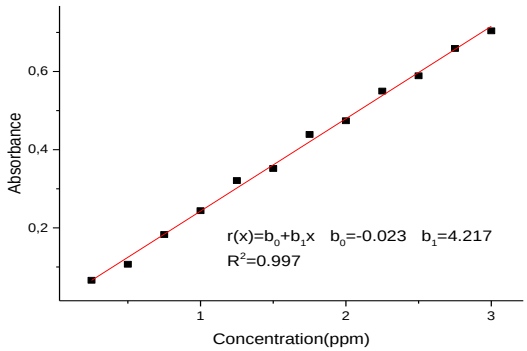

Figure 5: Calibration curve for CV solutions

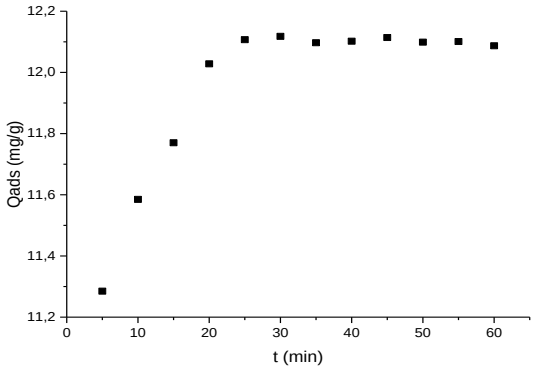

Figure 6: Amount of adsorbed of CV on SAN1 vs. time.

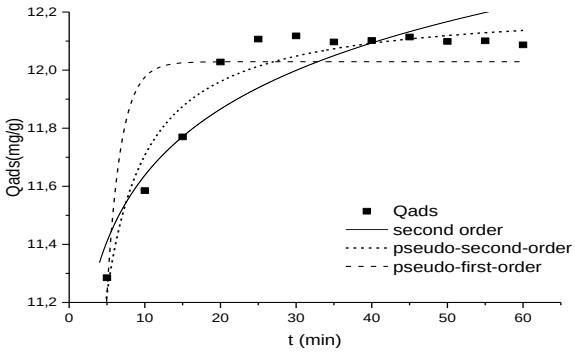

Figure 7: Kinetic models of pseudo-first, pseudo-second and second order

Adsorption isotherms

The experimental adsorption isotherm of CV in SAN1 is shown in Figure 8. The isotherm has been fitted to the Langmuir equation (R^2=0.99) (Table 5) reaching a q_{max} value of 55.63 mg/g. Therefore it was inferred that the adsorption takes place at specific sites of the adsorbent surface; considering that each site is occupied by a single adsorbate molecule and adsorption ceases once the material surface is saturated. The separation factor R_L for the CV adsorption in SAN was 0.3, indicating that the adsorption process is favorable. The strength of the interaction between adsorbent and adsorbate was carried out through desorption process at 373 K and later analysis in the UV spectrophotometer. In any case, it has been observed dye extraction of the adsorbent, which indicates the strong interaction between adsorbate and adsorbent.

Table 5: Calculated parameters from of the adsorption isotherms model of CV in SAN

Langmuir			**Freundlich**		
$q_{max}(mg/g)$	$k_L(mg/L)$	R^2	n	$k_f(mg/g)$	R^2
55.63	0.046	0.997	2.259	6.489	0.98

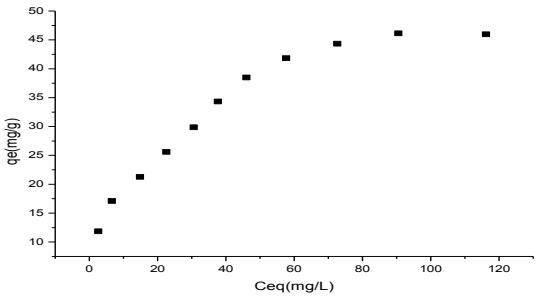

Figure 8: Experimental adsorption isotherm of CV in SAN1

In order to confirm the adsorption of CV in SAN, the raw mineral was recovered after the adsorption process and was evaluated by FTIR, elemental analysis (CNH) and XPS analysis. After the adsorption process, the FTIR spectrum (Figure 9) displays how new bands located at 1588, 1377 and 1169 cm^{-1} arise which is attributed to C=C stretching in aromatic nuclei, C-H deformation in methyl and C-H stretching in aromatic ring, respectively [33] confirming the adsorption of CV.

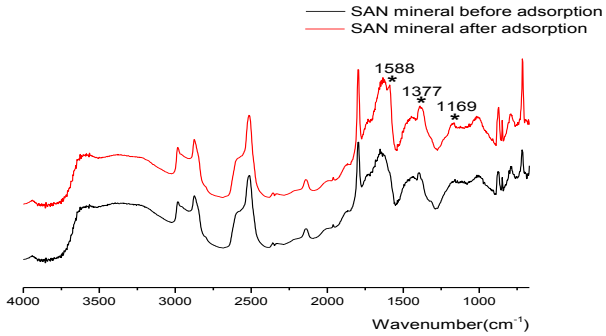

Figure 9: IR spectra before and after the adsorption process.

The elemental analysis (CNH) shows an increasing of the carbon content from 8.39 wt. % for the raw adsorbent to 8.78 wt.% for the SAN1 material after the adsorption process. In addition, it is noticeable the presence of a nitrogen content of 0.051 wt.% which also corroborates the adsorption of CV on the SAN1 mineral.
The XPS analysis of the mineral after the adsorption process (Table 3) shows how the carbon atomic concentration (%) increases as well as it arises a new contribution located at 287.2 eV attributed to C-N bonds. In addition, it appears a new signal in the N 1s region about 399.1eV attributed to -N-$(CH_3)_2$ [34]. Moreover, the other elements diminish their atomic concentration on the surface, which suggests the adsorption of the CV takes place on the surface of SAN1 mineral (Table 6).

Table 6: Adsorption capacities of various adsorbents materials and SAN

Crystal Violet		
Materials	Q_{ads}(mg/g)	Reference
activated sintering process red mud	60.5	[29]
Sulfuric acid-activated carbon	85.8	[30]
carAlg/MMt nanocomposite hydrogels	88.8	[31]
TiO_2-based nanosheet	58.3	[32]
Untreated rice bran	41.68	[32]
SAN	55.63	This Work

In order to elucidate if the adsorption process is attributed to the carbonate or aluminosilicate species, the SAN1 mineral was digested with HCl to remove the carbonate species of the mineral. The acid treatment leads to the loss of the material of 90 wt. %. The XRD of the treated material (Figure 2) confirms the absence of the typical diffraction peaks of carbonate species. This diffractogram reveals the existence of a natural zeolite (clinoptilolite), a mixture of feldspars and minor quantities of clay mineral and quartz. The acid treatment causes a slight increase of the specific surface area from 41 m^2/g for the SAN1Q mineral to 61 m^2/g for the SAN treated with HCl. This material maintains a type II isotherm with a H3 type hysteresis loop which is attributed to agglomerates of particles forming slit shaped pores (plates or edged particles like cubes) [27].

With regard to the FTIR spectrum of the SAN1Q treated with HCl (Figure 1b), the typical bands of carbonate species disappear, as was observed in the XRD data (Figure 2). This spectrum displays a broad band between 1300 and 900 cm^{-1} which is attributed to the Si-O stretching of the aluminosilicate material and a band close to 790 cm^{-1} ascribed to Al-O-Si in-plane vibration [25]. In addition, the broad band between 3700 and 3000 cm^{-1} is attributed to the symmetrical stretching vibration mode of O–H of the natural zeolite (clinoptilolite). Finally, the band about 1640 cm^{-1} is assigned to the bending vibration of the zeolitic water [25].

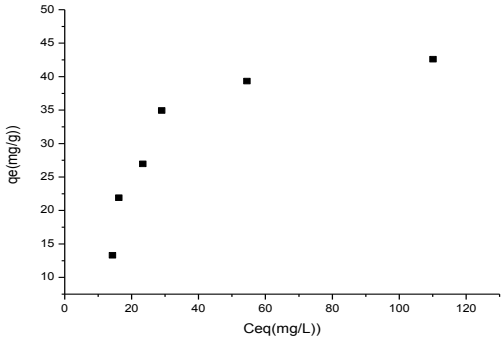

Figure 10: Experimental adsorption isotherm of CV in SAN1Q treated with HCl

The isotherm adsorption of the SAN1Q treated with HCl (Figure 10) displays a q_{max}=50.21 mg/g. This value is slightly lower than those obtained for SAN1 material. This fact indicates that the adsorption process is mainly attributed to the presence of rich-carbonate minerals such as calcite. It has reported in the literature that zeolite has a higher adsorption capacity, however the low specific surface area of the SAN1Q treated with HCl and the blockage of the active centers by the presence of water hinders the access of CV molecules to the active sites. It has been reported in the literature that the amine groups tends to be adsorbed on the negatively charged calcite surface suggesting that the adsorption process of the amine is mainly due to electrostatic attraction between the negative carbonate species and the positive ammonium ions [35]. A previous research about surface speciation of Ca and Mg carbonate minerals in aqueous solutions reported that the main carbonate surface species are $>CO_3^-$ (at pH> 5) and $>CO_3H^-$ (at pH <3) which confirms the negatively charged surface of the calcite [36].

CONCLUSIONS

1. SAN1 has proved to be a mineral with a high content of calcite mainly macroporous and with a relatively low specific surface.
2. Adsorption of CV by SAN1 was satisfactorily adjusted by the Langmuir model.
3. The kinetics of adsorption of CV by SAN1 is satisfactorily described by the pseudo-second order model.
4. The relatively high adsorption capacity for CV by SAN1: 55.63 mg/g, the speed of the process and the great availability of mineral, make it a good prospect for use in removing CV from aqueous solutions, especially when large volumes of contaminated water require to be treated.

REFERENCES

[1] UN 2014. Water for the world. United Nations. http://www.un.org/es/sustainablefuture/ water.shtml
[2] Allen SJ, Koumanova B. 2005. Decolourisation of water/wastewater using adsorption. J ChemTechnolMetall 40:175-92.
[3] Kumar R, Ahmad R 2011. Biosorption of hazardous crystal violet dye from aqueous solution onto treated ginger waste (TGW). Desalination 265: 112-118.
[4] Monash P, Pugazhenthi G 2009. Adsorption of crystal violet dye from aqueous solution using mesoporous materials synthesized at room temperature. Adsorption 15:390-405.
[5] http://www.inecc.gob.mx (citado el 10-06-2014)
[6] Srinivasan A, Viraraghavan T 2010. Decolorization of dye wastewaters by biosorbents: a review. J Environ Manage 91: 1915-1929.
[7] An S, Liu X, Yang L, Zhang L 2015. Enhancement removal of crystal violet dye using magnetic calcium ferrite nanoparticle: Study in single- and binary-solute systems. Chemical Engineering Research and Design 94:726-735.
[8] Oladipo AA, Gazi A 2014. Enhanced removal of crystal violet by low cost alginate/acid activated bentonite composite beads: Optimization and modelling using non-linear regression technique. J Water Proc Eng 2:43-52.
[9] Nandi BK, Goswami A, Purkait MK 2009. Removal of cationic dyes from aqueous solutions by kaolin: kinetic and equilibrium studies. Appl Clay Sci 42:583-590.

[10] Hameed BH 2009. Evaluation of papaya seeds as a novel non-conventional low-cost adsorbent for removal of methylene blue, J Hazard Mater 162: 939-944.
[11] Arami M, Limaee NY, Mahmoodi NM, Tabrizi NS 2005. Removal of dyes from colored textile wastewater by orange peel adsorbent: equilibrium and kinetic studies, J Colloid InterfSci 288: 371-376.
[12] Colectivo de autores. Rocas y minerales industriales de la República de Cuba. Instituto de Geología y Paleontología (IGP). La Habana, Cuba; 2011.
[13] Lagregren S 1898. About the Theory of So-Called Adsorption of Soluble Substances, Kungliga SvenskaVetenskap-sakademiensHandlinga 24:1-39.
[14] Ho YS. McKay G. 1999. Pseudo-Second-Order Model for Sorption Processes, Process Biochem 34:451-465.
[15] Chien SH, Clayton WR 1980. Application of Elovich Equation to the Kinetics of Phosphate Release and Sorptionon Soils, Soil Sci Soc Am J 44:265-268
[16] Salim MD, Munekage Y 2009. Lead Removal from Aqueous Solution Using Silica Ceramic: Adsorption Kinetics and Equilibrium Studies. Int J Chem 1: 23-30.
[17] Foo KY, Hameed B 2010. Review. Insights into the modeling of adsorption isotherm systems. ChemEng J 156:2-10.
[18] Dulman V, Cucu-Man SM 2009. Sorption of some textile dyes by beech wood sawdust. J Hazard Mater 162: 1457-1464.
[19] Gutiérrez-Segura E, Solache-Ríos M, Colín-Cruz A, Fall C 2012. Adsorption of cadmium by Na and Fe modified zeolitic tuffs and carbonaceous material from pyrolyzed sewage sludge. J Environ Manage 97: 6-13.
[20] Andersen FA, Brecevié LJ 1991. Infrared Spectra of Amorphous and Crystalline Calcium Carbonate.- ActaChemScand 45:1018-1024.
[21] Nakamoto K 1986. Infrared and Raman spectra of inorganic and coordination compounds, Ed. JonhWiley&Sons, New York.
[22] Correia LM, Saboya RMA, Campelo NS, Cecilia JA, Rodríguez-Castellón E, Cavalcante Jr. CL, Silveira RV 2014. Characterization of calcium oxide catalysts from natural sources and their applications in transesterification of sunflower oil. BioresourceTechnol 151:207-213.
[23] Ylmén R, Jäglid U 2013. Carbonation of Portland Cement Studied by Diffuse Reflection Fourier Transform Infrared Spectroscopy. Int. J. Concrete Struct Mater 7:119-125.
[24] Vagenas NV, Gatsouli A, Kontoyannis CG 2003. Quantitative analysis of synthetic calcium carbonate polymorphs using FT-IR spectroscopy. Talanta 59: 831-836.
[25] Madejova J, Komadel P 2001. Baseline studies of the clay minerals society source clays: Infrared methods. Clay Clay Miner 49:410-432
[26] Milovski AV, Konomov OV 1988. Mineralogía Edit. Mir. Moscow.
[27] Sing KSW 1985. Reporting physisorption data for gas/solid systems with special reference to the determination of surface area and porosityInternational. Pure ApplChem 57:603-619.
[28] Marsh M, Rodríguez-Reinoso F 2006. ActivatedCarbonElsevier. Chapter 8.
[29] Zhang L, Zhang H, Guo W, Tian Y 2014. Removal of malachite green and crystal violet cationic dyes from aqueous solution using activated sintering process red mud. Appl Clay Sci 93: 85-93.
[30] Senthilkumaar S, Kalaamani P, SubburaamCV 2006. Liquid phase adsorption of crystal violet onto activated carbons derived from male flowers of coconut tree. J Hazard Mater 136: 800-808.
[31] Mahdavinia GR, Aghaie H, Sheykhloie H, Vardini MT. Etemadi H 2013. Synthesis of CarAlg/MMt Nanocomposite Hydrogels and Adsorption of Cationic Crystal Violet. CarbohydPolym 98:358-365.
[32] Chen FT, Fang PF, Gao YP, Liu Z, Liu Y, Dai YQ 2012. Effective Removal of High-Chroma Crystal Violet over TiO_2-Based Nanosheet by Adsorption−Photocatalytic Degradation. Chem. Eng. J. 204:107-113.
[33] Bajpai SK, Jain A 2012. Equilibrium and Thermodynamic Studies for Adsorption of Crystal Violet onto Spent Tea Leaves (STL)Water J 4:52-71.
[34] Jones C, Sammann E(1990)The effect of low power plasmas on carbon fibre surfaces. Carbon 28:509-514.
[35] Andersen JB, El-Mofty SE. Somasundaran P 1991. Colloids Surface 55:365-368.
[36] Pokrovsky OS, Schott J, Thomas F, Mielczarski J 1998. Surface Speciation of Ca and Mg Carbonate Minerals in Aqueous Solutions: A Combined Potentiometric, Electrokinetic, and DRIFT Surface Spectroscopy Approach. Mineral Mag 62A:1196-1197.

INTERNATIONAL JOURNAL OF
PLANT, ANIMAL AND ENVIRONMENTAL SCIENCES

ISSN 2231-4490

International Journal of Plant, Animal and Environmental Sciences